https://doi.org/10.5194/egusphere-2025-4869
Preprint. Discussion started: 15 December 2025

Statistical characteristics of non-volcanic tremor distributions along the Mexican Subduction Zone

Quetzalcoatl Rodríguez-Pérez[1,2], Víctor H. Márquez-Ramírez[2], F. Ramón Zúñiga[2]

[1] Secretaría de Ciencia, Humanidades, Tecnología e Innovación, Mexico City, Mexico.
[2] Instituto de Geociencias, Universidad Nacional Autónoma de México, Juriquilla, Querétaro, Mexico.

Correspondence: Quetzalcoatl Rodríguez-Pérez (quetza@geociencias.unam.mx)

Abstract.

We analyze statistical characteristics of non-volcanic tremor sequences determined in the Mexican subduction zone. To achieve this objective, we used different techniques such as the Gutenberg-Richter relationship, non-extensive statistics, and the multifractal detrended moving average analysis to extract information on the magnitude and interevent-time distributions. The *b*-value results reveal that *b* fluctuates from 1.25 to 2.42, with the highest values corresponding to the plate interface down-dip regions. On the other hand, the *q*-value shows an inverse behavior, having the highest values in the inter-plate coupling region. Similar to tectonic earthquakes, the non-volcanic tremor sequences show a multifractal structure in magnitude and interevent data. The multifractality analysis suggests that multifractality may be associated with long-term correlations, the probability distribution of the data, and the presence of nonlinearities. Regarding the existence of apparent and intrinsic multifractality, our results indicate that both sources are present in the sequences, with the former being the most common. Our estimates of the Hurst exponent are in the interval of 0.65 to 1.06, with the majority indicating an exceptionally high persistent memory ($H > 0.95$). With respect to the estimation of the distribution that better describes the interevent sequences, we find that most sequences can be described by a Lognormal distribution and, to a lesser extent, by a Gamma distribution. Our investigation also showed that observations of the duration of tectonic tremors present a large scatter, resulting in scaling

https://doi.org/10.5194/egusphere-2025-4869
Preprint. Discussion started: 15 December 2025

relationships with low values of the determination coefficient. The source of this variability may be related to the generation mechanism of NVT or to the process of detection and description of the signals.

Keywords Non-volcanic tremor, *b*-value, non-extensive statistics, multifractality, Mexico

1 Introduction

Non-volcanic tremor (NVT) is an enigmatic seismic phenomenon that has become a relevant topic of study, mainly in subduction zones. NVTs are emergent seismic signals of long duration and low amplitude (Obara, 2002). Previous studies have shown that NVTs are composed of repeating small low-frequency earthquakes, commonly accompanied by very-low-frequency earthquakes that, in both cases, involve shear failure and slip (Shelly et al., 2007; Bostock et al., 2015; Gomberg et al., 2016a, b). NVTs mainly occur within the plate interface close to the shallow and deep edges locked regions. This phenomenon can also be observed in other tectonic environments, such as in convergent regions (e.g., Taiwan, Tang et al., 2010) or continental transform zones (e.g., California, Nadeau and Dolenc, 2005; Shelly, 2010). Fluids are implicated in generating NVTs in a similar form to regular volcanic tremors (Obara, 2002). Pressure and temperature conditions at subduction zones, in addition to dehydration, control the occurrence of NVT (Yoshioka et al., 2008; Peacock, 2009). It has been reported that NVTs occur in regions of high pore-fluid pressure (Shelly et al., 2006). Other factors are important in generating tectonic tremors, such as the material composition in the overriding plate above the tremor zone in the wedge mantle and the metamorphism of subducting seamounts (Wada et al., 2008). Non-volcanic tremors commonly exhibit episodic activity, with periods of intense activity lasting from days to weeks, interrupted by periods of scarce activity that last for months, during which there are few or no tremor episodes (Obara, 2002). Regularly, NVTs coexist with slow earthquakes; both phenomena share

https://doi.org/10.5194/egusphere-2025-4869
Preprint. Discussion started: 15 December 2025

temporal and spatial occurrence (Rogers and Dragert, 2003). Another important feature of NVTs is that they can be triggered by large earthquakes, such as the case of the 2002 Denali earthquake (M_W = 7.8) in Alaska (Rubinstein et al., 2007) and the 2003 Takachi-oki earthquake (M_W = 8.1) in Japan (Miyazawa and Mori, 2005), in both cases these earthquakes, activated NVT activity.

Tectonic tremors have been reported along the Middle America Trench in Mexico in Guerrero (Payero et al., 2008; Cruz-Atienza et al., 2015; Villafuerte and Cruz-Atienza, 2017; Husker et al., 2019; Plata-Martínez et al., 2021; Chen et al., 2025), Jalisco-Colima (Ide, 2012), and Oaxaca (Brudzinski et al., 2010; Husker et al., 2019) states. In Guerrero, NVTs have been detected at about 200 km downdip, at depths of 40-50 km, and within a few kilometers from the trench, at depths of 10-16 km (Plata-Martínez et al., 2021; Chen et al., 2025). Similar to the Guerrero case, in Oaxaca, NVTs are located approximately 150-200 km from the trench at depths of 30-50 km (Brudzinski et al., 2010). On the other hand, in Western Mexico, NVTs occur in a narrow band oriented parallel to the trench, mostly at depths of 30-50 km (Ide, 2012). Much of the effort in studying tectonic tremors is directed toward locating events, generating catalogs, and their tectonic interpretation. Few studies have focused on determining the statistical characteristics of event occurrence. For example, Kao et al. (2010) determined the *b*-value of NVT sequences in northern Cascadia (M_W ~1.0 - 1.7), finding that the *b*-value appears to be 1. Staudenmaier et al. (2019) estimated the *b*-value of NVTs in the San Andreas Fault ($0.44 < M_W < 2.7$), obtaining a *b*-value of 2.52. In contrast, other studies reported extremely high *b*-values ($b > 5$ with $1.5 < M_W < 2.7$; $b = 4.2$ with $0.3 < M_W < 1.5$) (Sweet et al., 2014; Bostock et al., 2015). In this article, we studied the statistical features of NVT sequences generated at the Mexican subduction zone. We analyzed the Gutenberg-Richter relationship, non-extensive statistics, and multifractality of magnitude and interevent-time distributions. Our results characterize particular statistical information of NVTs associated to subduction zones which may help shade light on their

https://doi.org/10.5194/egusphere-2025-4869
Preprint. Discussion started: 15 December 2025

generation.

2 Tectonic setting

The Mexican subduction zone (MSZ) is located along the border of three tectonic plates: the Cocos (CO), North American (NA), and Rivera (RI) plates, respectively (Fig. 1). Convergence rates predicted from the NUVEL1-A model (DeMets et al., 1994) fluctuate from 2.0 to 6.8 cm/yr for the RI-NA convergence in the north (Jalisco-Colima) to the CO-NA convergence in the south (Oaxaca), respectively (Fig. 1). The rupture areas of the previous largest earthquakes exhibit a seismic gap in the MSZ, known as the Guerrero seismic gap (GG). The GG is a 200 km long segment in the CO-NA plate boundary (Fig. 1). The gap is capable of producing an earthquake with a magnitude of 8.1-8.4 if the entire gap were ruptured in a single event (Singh and Mortera, 1991). The gap has not experienced a significant event ($M > 7$) since 1911. The geometry of the subducted slab varies from north to south. In the Jalisco region, the RI plate subducts at a steep angle (~ 50º), and then the dip angle of the CO plate decreases gradually toward the southeast. In the Gurrero-Oaxaca region, the subducted slab is almost subhorizontal (Pardo and Suárez, 1995; Pérez-Campos et al., 2008). As mentioned above, non-volcanic tremors occur at certain regions within the subduction zone regime. They appear to signal the transition from creep to locking trench parallel segments (Chen et al., 2025).

3 Data and methods

3.1 Data

We retrieved non-volcanic tremor catalogs for events from six different sequences along the Mexican subduction zone, as reported in previous studies (Ide, 2012; Idehara et al., 2014; Husker et al., 2019; Plata-Martínez et al., 2021; Chen et al., 2025). We studied NVT events from 2005 to 2019, with hypocentral depths lower than 50 km and magnitudes ranging from -0.8 to 3.65 (Table 1). Sequences 1,

https://doi.org/10.5194/egusphere-2025-4869
Preprint. Discussion started: 15 December 2025

3 and 4 took place down dip from the coupling plate interface of the Guerrero segment. Sequences 5 and 6 occurred at the coupling plate interface of that segment. Sequence 2 was located further west, at the boundary between the subduction regimes of Rivera and Cocos plates (Fig. 2). The information reported in these catalogs is the following: origin time, hypocentral location, moment magnitude (M_W), and time duration for sequences 1 to 3 and 5. In the case of sequence 4, locations were performed by single local seismic stations, resulting in only information about origin time and hypocentral location. Similar to the previous case, in sequence 6, event magnitudes are not reported. Although magnitudes are not available for sequences 4 and 6, these catalogs contain sufficient information to study the interevent time. Hypocenters of NVTs were located in the States of Guerrero and Jalisco and were detected mainly through temporal seismic networks (Sequences 1, 2, 3, 5, and 6).

3.2 Methods

3.2.1 Estimation of the *b*-value

The earthquake frequency-magnitude distribution (FMD) is commonly described by the Gutenberg-Richter law (Gutenberg and Richter, 1944):

$$\log_{10} N(M) = a + bM \quad , \tag{1}$$

where N is the number of earthquakes $\geq M$ above the magnitude of completeness (M_c), a and b are constants that describe the earthquake productivity and the proportion of small to large events, respectively. Globally, the b-value is about one on average (Lay and Wallace, 1995). Fluctuations from this value are due to several factors, such as fluid pressure (Henderson et al., 1994), heterogeneity in the fault zone (Mogi, 1963), thermal gradient (Warren and Latham, 1970), variations in the state of stress (Schorlemmer et al., 2005; Scholz, 2015). The b-value is determined using the maximum

https://doi.org/10.5194/egusphere-2025-4869
Preprint. Discussion started: 15 December 2025

likelihood method proposed by Aki (1965). The equation that describes this estimator is the following

$$b = \frac{\log_{10} e}{\bar{M} - \left(M_c - \Delta M/2\right)} \quad , \tag{2}$$

where M_c is the catalog completeness magnitude, $\bar{M}$ is the average magnitude with a magnitude greater than M_c, and ΔM is the magnitude binning interval. We determined *b*-values for NVT sequences with reported magnitudes (sequences 1 to 3, and 5), the results are shown in Fig. 3 and Table 2.

3.2.2 Non-extensive statistical analysis

Non-extensive statistical mechanics (NESM) is a theoretical framework for analyzing non-equilibrium complex systems, such as earthquake phenomena. In the case of systems showing long-range correlations, memory, or fractal properties, NESM becomes the most suitable mathematical framework (Tsallis, 2009). In that context, Sotolongo-Costa and Posadas (2004) introduced the fragment asperity model. In this model, the release of seismic energy (ε) is associated with the size of *r* fragments filling the space between irregular fault interfaces. Silva et al. (2006) used a volumetric relationship between seismic energy and fragment size in the form of $\varepsilon \propto r^3$, under this assumption, the cumulative distribution of the number of earthquakes *N* with a magnitude greater than *M* is

$$\log \frac{N>M}{N} = \frac{(2-q)}{(1-q)} \log\left[1 - \left(\frac{1-q}{2-q}\right)\left(\frac{10^{2M}}{a_s^{(2/3)}}\right)\right] \quad , \tag{3}$$

where the *q*-value is in the range of $1 < q < 2$, the constant a_s is a proportionality parameter between the released seismic energy and the fragment size. The *q*-value measures the length scale of spatial

https://doi.org/10.5194/egusphere-2025-4869
Preprint. Discussion started: 15 December 2025

interactions; a q-value of ~ 1 indicates short-ranged spatial correlations, and as q increases, the physical state becomes increasingly unstable. High q-values indicate that the fault planes are not in equilibrium, and more events can be expected (Sotolongo-Costa and Posadas, 2002). In most tectonic regimes, q varies from 1.5 to 1.7 (Sarlis et al., 2010). We calculated the q-values of all NVT sequences with reported magnitudes. The results are shown in Fig. 4 and Table 3.

3.2.3 Multifractal detrended moving average analysis

The multifractal detrended fluctuation analysis (MFDFA) is a technique that quantifies the dynamic structure of a time series (Kantelhardt et al., 2002). An improvement of the MFDFA was presented by Gu and Zhou (2010), known as multifractal detrended moving average analysis (MFDMA). We employ the MFDMA technique to investigate the multifractal properties of interevent time and magnitude distributions of NVT sequences. We summarize the MFDMA algorithm of Gu and Zhou (2010) as follows. First, a cumulative time series of a given physical parameter $M(t)$ is constructed and represented as

$$y(t)=\sum_{i=1}^{t} M(i) \quad , \tag{4}$$

where t = 1, 2, 3, …, N (length of the time series) and $M(i)$ is the observed time series. Then, a moving average function of $y(t)$ is calculated in a moving window as

$$\tilde{y}=\frac{1}{s}\sum_{k=-1\lfloor(s-1)\theta\rfloor}^{\lceil(s-1)(1-\theta)\rceil} y(t-k) \quad , \tag{5}$$

https://doi.org/10.5194/egusphere-2025-4869
Preprint. Discussion started: 15 December 2025

where s is the window size, $\lfloor x \rfloor$ is the largest integer not greater than argument x, $\lceil x \rceil$ is the smallest integer not smaller than argument x, and θ is the position index which describes the delay between the moving average function and the original time series ($0 < \theta < 1$). For example, if $\theta = 0$, 0.5, and 1, it describes a backward, centered, and forward moving average, respectively.

Afterwards, the residual sequences are obtained by detrending the time series through removing the average function, $\tilde{y}(i)$, resulting in

$$(i) = y(i) - \tilde{y}(i) \quad , \tag{6}$$

where $s \le i \le N$. The residual series ((i)) is divided into N_s disjoint segments with the same size of s, where $N_s = N/s - 1$. The residual sequence for each segment is denoted by $_v$, where $_v(i) = (l+i)$ for $1 \le i \le s$ and $l = (v-1)s$. Then we calculate the root-mean-square fluctuation function ($F_v(s)$) for a segment of size s as follows

$$F_v(s) = \left\{ \frac{1}{s} \sum_{i=1}^{s} {}^{2}_{v}(i) \right\}^{1/2} \quad . \tag{7}$$

The q-th order fluctuation function ($F_q(s)$) is obtained by

$$F_q(s) = \left\{ \frac{1}{N_s} \sum_{v=1}^{N_s} F_v^q(s) \right\}^{1/q} \quad , \tag{8}$$

for all $q \neq 0$. For the case of $q = 0$, we have

https://doi.org/10.5194/egusphere-2025-4869
Preprint. Discussion started: 15 December 2025

$$\ln\left[F_0(n)\right]=\frac{1}{N_n}\sum_{\nu=1}^{N_s}\ln\left[F_\nu(s)\right] \quad , \tag{9}$$

where the scaling behavior of $F_q(s)$ follows the relation that is given by $F_q(s) \sim s^{h(q)}$ where $h(q)$ is the Holder exponent or generalized Hurst exponent. The multifractal scaling exponent is calculated by

$$\tau(q)=q\,h(q)-1 \quad . \tag{10}$$

Finally, the singularity strength function ($\alpha(q)$) and the multifractal spectrum ($f(\alpha)$) can be obtained as

$$\alpha(q)=\frac{d\,\tau(q)}{dq} \quad , \tag{11}$$

and

$$f(\alpha)=q\,\alpha-\tau(q) \quad , \tag{12}$$

respectively. In the multifractal analysis of sequences 1 to 4, we used the following input parameters: N = 30, θ = 0, $q\in[-5,5]$ with q increments of 0.2, the lower bound of segment size s is fixed to 10, while the upper bound is given by $N/10$, as recommended by Gu and Zhou (2010). In the case of sequences 4 and 5, the upper bound of segment size s is set to $N/4$ because they have less data than the other sequences. Results for $F_q(s)$, $h(q)$, $\tau(q)$, $\alpha(q)$, and $f(\alpha)$ for interevent time and magnitude distributions are shown in Figs. 5 and 6 and Figs. 7 to 9, respectively.

https://doi.org/10.5194/egusphere-2025-4869
Preprint. Discussion started: 15 December 2025

3.2.4 Multifractal parameters

We determined multifractal parameters using the equations presented in the previous section, following De Freitas and França (2024). We start with the degree of asymmetry (A), defined as

$$A = \frac{\alpha_{max} - \alpha_0}{\alpha_0 - \alpha_{min}} \quad , \tag{13}$$

where α_0 is the value for which $f(\alpha)$ is maximum. If $A = 1$, $f(\alpha)$ is symmetric. On the contrary, when $A > 1$, the symmetry is right-skewed, and if $0 < A < 1$, the symmetry is left-skewed. The values of α_{max} and α_{min} represent the extreme values of the singularity exponent and are related to the minimum and maximum fluctuation of the signal. The degree of multifractality ($\Delta\alpha$), which is determined by

$$\Delta\alpha = \alpha_{max} - \alpha_{min} \quad . \tag{14}$$

A low value of $\Delta\alpha$ denotes that the time series is close to fractal. On the other hand, a high value of $\Delta\alpha$ indicates that the multifractal strength is higher (De Freitas and De Medeiros, 2009). The singularity parameter (Δf) describes the broadness of the singularity spectrum and is defined as

$$\Delta f = f(\alpha_{max}) - f(\alpha_{min}) \quad . \tag{15}$$

In the case that $\Delta f > 1$, the left-hand side is less deep, while if $\Delta f = 0$, both depths of the tails are equal. According to Ihlen (2012), a long left tail indicates that the singularities are stronger, while in contrast, a long right tail indicates that the singularities are weaker. The Hurst index (H) can be obtained from

https://doi.org/10.5194/egusphere-2025-4869
Preprint. Discussion started: 15 December 2025

the multifractal spectrum through the second-order generalized Hurst exponent $h(q = 2)$. If is $H > 0.5$, it indicates persistence in long-range correlation, while $H \approx 0.5$ shows a random character of the series (past and future fluctuations are uncorrelated or Brownian motion). On the other hand, $H < 0.5$ reflects anti-persistence. In this case, the fluctuations tend not to continue in the same direction, but instead turn back on themselves, resulting in a less smooth time series (Hampson and Mallen, 2011).

3.2.5 Sources of multifractality

Multifractality can be classified into two categories: apparent and intrinsic. The former type refers to the multifractality that arises from spurious patterns, while the latter refers to the genuine source derived from nonlinear processes within the data (Saichev and Sornette, 2006). The differentiation between apparent and intrinsic multifractality is critical for understanding the process present in a time series (Jiang et al., 2019). On the other hand, there are three primary sources for multifractality in time series: 1) the non-Gaussian distribution of innovations, 2) the linear long-range correlations, and 3) the nonlinear long-range correlations (Jiang et al., 2019; Wang, 2023). Two methods are commonly used to investigate the source of multifractality: shuffling and surrogating procedures, respectively. These methods involve modifying the original sample to eliminate the source of multifractality. Dealing with the first source of multifractality is achieved through shuffled time series. The random shuffling of a time series removes linear and nonlinear temporal correlations (a possible reason for the scaling of F_q) while the probability distribution (PDF) remains unchanged (Kantelhardt, 2009). Thus, if F_q from the shuffled series scales in the same way as those from the original series, one may assume that the scaling must be due to the probability distribution of the data. If the shuffled series exhibits weaker multifractality compared to the original data, then we can assume that multifractality stems from both temporal correlation and PDF. Consequently, if no multifractal feature remains after performing the shuffling procedure on the original series, we can interpret that long-range correlation dominates the

https://doi.org/10.5194/egusphere-2025-4869
Preprint. Discussion started: 15 December 2025

multifractality in the original series.

The surrogate time series method generates time series via a Fourier transform, preserving amplitudes but randomizing the phases, and then performs an inverse Fourier transform. In this form, non-linearities in the series are eliminated while preserving long-range correlations. The iterated amplitude-adjusted Fourier Transform (IAAFT) algorithm (Schreiber and Schmitz, 1996; 2000) is appropriate for this purpose. With the surrogate series, we performed statistical tests for $h(q)$, $\tau(q)$, $\alpha(q)$, and $f(\alpha)$ to determine the presence or absence of intrinsic multifractality in the data. For this purpose, the tests consist of determining if the indicator is greater than the indicator derived from the IAAFT series; in other words, we need to calculate the probability that x is smaller than x_{IAAFT} (p-value = $Pr(x < x_{IAAFT})$), where x is a multifractal indicator, as proposed by Wang et al. (2023). Wang et al. (2023) also stated that if the p-value is smaller than a significance level (usually 5%), then we can reject the hypothesis that the original time series is monofractal. The low p-values also suggest that the original time series may have an intrinsic multifractal nature beyond the fat-tailedness and potential long-term linear correlations. Alternatively, high p-values suggest the absence of intrinsic multifractality (De Freitas and França, 2024). Here, we applied the MFDFA to the magnitude and interevent time series of NVT. In both cases, we generated 100 shuffled and IAAFT surrogate time series and calculated the multifractal indicators to analyze the source of multifractality. We used surrogate data to test the presence of intrinsic multifractality in the time series. The results are presented in Figs. 5 to 9 and Table 4.

3.2.6 Interevent-time distribution and duration scaling

Several interevent-time distributions have been proposed in the literature to explain interevent earthquake observations (e.g., Gamma, Exponential, Lognormal, Weibull) (Corral, 2006; Davidsen and Kwiatek, 2013). We fitted interevent time data from all the NVT sequences, considering the previously

https://doi.org/10.5194/egusphere-2025-4869
Preprint. Discussion started: 15 December 2025

mentioned statistical distributions, using the maximum likelihood estimation method as described by Mesimeri et al. (2019). To discern the best goodness of fit, we applied a Kolmogorov-Smirnov test. The Akaike and Bayesian information criteria (AIC and BIC, respectively) were also calculated to test the relative quality of the statistical models. The best-fitted distribution is the one with the lowest AIC and BIC values. The obtained interevent-time probability distributions are shown in Fig. 10 and Table 5. Additionally, we determined scaling relationships between the tremor duration and magnitude for sequences 1 to 3 and 5. The obtained scaling relations have the following form:

$$\log(\tau) = \alpha M_W + \beta \quad , \tag{16}$$

where τ is the duration of the NVT, M_W is the moment magnitude, and α and β are constants. We present the estimated scaling relationships in Fig. 11 and Table 5.

4 Results

Our estimates of the *b*-value showed that *b* for NVTs at the Mexican subduction zone is in the range of 1.25 – 2.42 with completeness magnitudes between 1.10 and 1.80. Sequences 1 and 3 have the highest *b*-values, indicating a possible individual feature of the down-dip Guerrero segment of the Cocos plate. They are followed by sequence 2, located at the interface between the Rivera and Cocos plates. The lowest *b*-value is found for sequence 5 in the Guerrero Gap region (Fig. 2 and Table 2), which unfortunately can not be corroborated with sequence 6 at the same region since it does not include magnitude data. The *q*-value from the non-extensive statistical analysis fluctuates from 1.39 to 1.65. They show an apparent inverse relation with the *b*-value behavior since the sequences located near the trench (2 and 5) indicate higher *q*-values than those located down-dip (1 and 3) with identical *q*-values. Multifractal indicators of the original time series show that the multifractal spectra are mostly right-

https://doi.org/10.5194/egusphere-2025-4869
Preprint. Discussion started: 15 December 2025

skewed (magnitude sequences 1 to 4, interevent time sequences 1, 2, and 6). In contrast, left-skewed spectra correspond to interevent time sequences 3 and 4. Sequence 5 exhibits a symmetric multifractal spectrum. Results for the degree of multifractality ($\Delta\alpha$) indicate that interevent time series have a higher multifractal strength than magnitude time series. On the other hand, the singularity parameter (Δf) indicates that the singularities are weaker for magnitude sequences 2 and 3, as well as interevent time sequences 1-2 and 6. Contrarily, the singularities are stronger for interevent time sequences 3 and 4. Estimates of the Hurst exponent depict a long-term persistence signature ($H > 0.5$).

By comparing the multifractality spectra ($Fq(s)$, $h(q)$, $\tau(q)$, $\alpha(q)$, and $f(\alpha)$) of shuffled and surrogates procedures, we observe that they can not destroy the multifractality, indicating that long-term correlations, the probability distribution of the data, and the presence of nonlinearities are present in the NVT time sequences. The statistical test results for surrogate data showed that *p*-values for multifractal indicators (A, $\Delta\alpha$, Δf, and H) indicate that magnitude sequence five and interevent time sequences 1, 4, and 5 exhibit apparent multifractality due to relatively high *p*-values. On the contrary, low *p*-values of multifractal parameters for magnitude sequence 1 suggest the presence of intrinsic multifractality. In the cases of magnitude sequences 2 and 3, and interevent time sequences 2, 3, and 6, *p*-values related to multifractal indicators are inconclusive for determining the nature of multifractality because half of the indicators exhibit low *p*-values, while the other half exhibit high values. Regarding the inter-event time distributions, a comparison between the fitted PDFs and the empirical ones from sequences 1 to 4 showed that the Lognormal distribution provides the best fit. In contrast, for sequences 5 and 6, the Gamma distribution yields the best fit for the interevent time data. In all cases, the least well-fitting distribution is the Exponential distribution (Fig. 10 and Table 5). Finally, event duration observations exhibit large scatter, resulting in linear scaling relationships with low determination coefficients ($0.03 < R^2 < 0.34$) (Fig. 11 and Table 6). This scatter is inherent to the genesis of NVT or is associated with the

https://doi.org/10.5194/egusphere-2025-4869
Preprint. Discussion started: 15 December 2025

detection process since it is present in all reported sequences.

5 Discussion

We start the discussion by comparing our *b*-value estimates with previous studies. The *b*-value associated with NVTs has been determined in crustal and subduction environments, with the latter being the most common. In crustal regions, for example, in the San Andreas Fault at the Parkfield segment, Staudenmaier et al. (2019) calculated a *b*-value of 2.52 for NVT episodes. For the case of subduction zones, it has been found that the *b*-value of NVTs fluctuates between 1.0 and 5 (Kao et al., 2010; Rabbel et al., 2011; Gallego et al., 2013; Sweet et al., 2014; Bostock et al., 2015). The Cascadia subduction zone, in Vancouver Island, exhibits both low and high *b*-values ($b \sim 1$ and $4.2 < b < 5$, respectively) (Kao et al., 2010; Sweet et al., 2014; Bostock et al., 2015). In Chile, the *b*-value of NVT sequences was determined as 2.4 (Gallego et al., 2013). Regarding *b*-value estimations of NVTs at the Cocos plate, Rabbel et al. (2011) estimated a value of 1 in the region of Costa Rica. Our results show that the *b*-value varies from 1.25 to 2.42 for the NVTs detected at the Mexican subduction regimes studied. We observed that in the down-dip segment, NVT sequences have the highest *b*-values (2.22-2.42), while in the inter-plate coupling region, the *b*-value is in the range of 1.25 – 1.41 (Table 2). The high *b*-values can be evidence of a larger degree of fracturing since they convey a larger proportion of small magnitude fractures as compared to larger ones. In general, the *b*-values obtained for the coupling region do not depart much from common tectonic events' *b*-value estimations. For example, for the Cocos plate, the *b*-value for tectonic seismic events has been observed to lie in the interval of 0.8 – 1.3 (Nishikawa and Ide, 2014). In terms of the non-extensive statistical analysis, our estimates of the *q*-value for NVT in Mexico are consistent with reports of *q*-value at subduction zones in which values of *q* fluctuate from 1.61 to 1.69 (Scherrer et al., 2015). These reports agree with our results, in which the *q*-value varies from 1.64 to 1.65. Our results also showed that interplate down-dip sequences have

https://doi.org/10.5194/egusphere-2025-4869
Preprint. Discussion started: 15 December 2025

lower *q*-values (1.39) (Table 3). High *q*-values of coastal regions can be explained by stress heterogeneity due to plate coupling and asperity distribution compared to interplate down-dip regions with different conditions, such as pressure, temperature, and rock structure.

Regarding the multifractal analysis, our results indicate that both magnitude and interevent time NVT sequences of NVT exhibit a multifractal structure, in a similar form to tectonic earthquakes (interevent time, Michas et al., 2015; magnitude, De Freitas and França, 2024). In relation to the identification of intrinsic multifractality, the tests of surrogate data verify that only one sequence exhibits intrinsic multifractality. On the contrary, four sequences confirm the presence of apparent multifractality, while in five sequences, the results are not conclusive. De Freitas and França (2024) also reported that the seismicity of some subduction zones has apparent multifractality, while others exhibit intrinsic multifractality. These observations agree with our findings. Conversely, our estimates of the Hurst exponent showed that H varies from 0.65 to 1.06. Most of the NVT sequences exhibit an exceptionally high persistent memory ($H > 0.95$) (Table 4). According to Cisternas et al. (2004), high H values may be associated with the volumes around the ruptured faults. Here, we interpreted high Hurst exponents as the result of the relatively limited volume of perturbed regions where the fluids are present. Our results are also in agreement with Hurst exponent reports for regional seismicity and aftershock sequences. For example, in southern Italy, Telesca et al. (2001) determined that H fluctuates from 0.5 to 0.92; in Taiwan and Greece, H is about 0.8 (Chen et al., 2008; Gkarlaouni et al., 2017, respectively), while in the San Andes fault zone in California, H is equal to 0.87 (De Freitas et al., 2013). In the case of the aftershocks of the 1999 Izmit earthquake (M_W = 7.6), the Hurst exponent has a value of 0.95 (Cisternas et al., 2004).

The interevent time analysis showed that NVT sequences 1 to 4 are well approximated by a Lognormal

https://doi.org/10.5194/egusphere-2025-4869
Preprint. Discussion started: 15 December 2025

distribution, while for sequences 5 and 6, by a Gamma distribution (Table 5). This shows that the inter-event time distributions exhibit a mixed behavior, with characteristics compatible with tectonic earthquakes and volcanic seismicity. For example, Traversa and Grasso (2010) showed that a Gamma distribution can mainly describe volcano seismicity, but some episodes reject the Gamma distribution to describe the seismic activity. In the case of the tectonic activity, several inter-event time density distributions have been proposed, such as the Exponential, Gamma, Lognormal, etc (Corral, 2006; Passarelli et al., 2015; Post et al., 2021). Our results are also consistent with global ($M_W \geq 7$, Bantidi, 2022) and regional ($0.1 < M_L < 5.1$, Mesimeri et al., 2019) seismicity studies, in which Lognormal fits best the interevent time observations. Additionally, our results depict a differentiated behavior between the down-dip and the interplate coupling regions. In the last case, the Gamma distribution is highlighted as explaining the observations better, possibly due to the smaller sample size (Table 1). Finally, the obtained event duration scaling relationships for all the NVT sequences exhibit large scatter. The data variability may be inherent to the genesis of NVT or be associated with the detection process since it is present in all reported sequences. It is a fact that tremors do not have clear phase arrivals, resulting in longer durations. On the other hand, determining reliable tremor parameters such as location, magnitude, peak amplitudes, and duration is challenging compared to regular earthquakes (Staudenmaier et al., 2019). The studied data highlight that the duration of the events varies from tremor episodes, even in the same subduction zone. According to Schwartz and Rokosky (2007), the mechanism that controls the duration and amplitude of tremors is not clearly known, but it is suggested that the presence of fluids may explain the tremor source. Although the relationship between slow earthquakes and tectonic tremors is not known with certainty, there is evidence that NVTs are modulated for slow dislocations on the plate interface (Villafuerte and Cruz-Atienza, 2017).

https://doi.org/10.5194/egusphere-2025-4869
Preprint. Discussion started: 15 December 2025

6 Conclusions

We studied statistical features of reported NVT sequences along the Mexican subduction zone. We analyzed the Gutenberg-Richter relation, non-extensive statistics, and multifractal properties of magnitude and interevent time series. We observed that *b*-values are in the range of 1.25 – 2.42, being consistent with reports worldwide. In particular, down-dip region NVT sequences have the highest *b*-values. In contrast, *q*-values of down-dip regions have lower values than those from coastal areas ($1.39 < q < 1.65$). Both magnitude and interevent time sequences exhibit multifractality, similarly to tectonic earthquakes, that may be related to long-term correlations, the probability distribution of the data, and the presence of nonlinearities. By analyzing surrogate data, we observed that some sequences exhibit apparent multifractality, and to a lesser extent intrinsic multifractality, although in other cases the criteria were not conclusive. Regarding the study of the PDFs, we find that most sequences can be described by a Lognormal distribution and in two cases by a Gamma distribution. This suggests that NVT sequences exhibit a mixed behavior with characteristics similar to tectonic earthquakes and volcanic seismicity. Concerning the NVT duration observations, a large scatter is observed, resulting in linear scaling relations with low determination coefficients. The variability in NVT durations may reflect an inherent origin or may be associated with the difficulties in the detection process and/or waveform parameter estimations.

Code availability. Estimations of *b*-value were performed with the Python code Calc_gr_ks (https://github.com/nadavwetzler/b-value; Wetzler, 2022). We calculate the interevent-time distributions with the code qks_statistics (https://github.com/mmesim/qks_statistics; Mesimeri, 2021). The MFDMA method was implemented with the code GFGU_MFDMA_1D (Gu and Zhou, 2010). MATLAB Chaotic Systems Toolbox for implementing shuffle and IAAFT surrogate time series are available at https://github.com/nmitrou/Simulations/tree/master/matlab_codes (Leontitsis, 2001).

https://doi.org/10.5194/egusphere-2025-4869
Preprint. Discussion started: 15 December 2025

Linear regressions for NVT duration scaling relations were determined with the SciPy library (Virtanen et al., 2020). Some figures were produced with Generic Mapping Tools (GMT) (Wessel et al., 2019). In all cases, last access: September 2025.

Data availability. NVT catalogs for sequences 1 to 3 were taken from the World Tremor Database (http://www-solid.eps.s.u-tokyo.ac.jp/~idehara/wtd0/Welcome.html, Ide, 2012; Idehara et al., 2014). Catalogs for sequences 4, 5, and 6 were obtained from Husker et al. (2019), Plata-Martínez et al. (2021), and Chen et al. (2025), respectively. In all cases, last access: September 2025.

Author contributions. Conceptualization: QRP. Data analysis: QRP, VHMR, FRZ. Writing and discussion of the manuscript: QRP, VHMR, FRZ.

Competing interests. The contact author has declared that none of the authors has any competing interests.

Financial support. QRP was supported by the Secretaría de Ciencia, Humanidades, Tecnología e Innovación (SECIHTI) (project 7197).

References

Aki, K.: Maximum likelihood estimate of b in the formula log $N = a - bM$ and its confidence limits, Bull. Earthq. Res. Inst., Univ. Tokyo 43, 237-239, 1965.

Bantidi, T.M.: Inter-occurrence time statistics of successive large earthquakes: analyses of the global CMT dataset, Acta Geophys., 70, 2603–2619, https://doi.org/10.1007/s11600-022-00908-2, 2022.

https://doi.org/10.5194/egusphere-2025-4869
Preprint. Discussion started: 15 December 2025

Bostock, M. G., Thomas, A. M., Savard, G., Chuang, L., and Rubin, A. M.: Magnitudes and moment-duration scaling of low-frequency earthquakes beneath southern Vancouver Island, J. Geophys. Res., 120, 6329-6350, https://doi.org/10.1002/2015JB012195, 2015.

Brudzinski, M. R., Hinojosa-Prieto, H. R., Schlanser, K. M., Cabral-Cano, E., Arciniega-Ceballos, A., Diaz-Molina, O., and DeMets, C.: Nonvolcanic tremor along the Oaxaca segment of the Middle America subduction zone, J. Geophys. Res., 115, B00A23, https://doi.org/10.1029/2008JB006061, 2010.

Chen, C.-C., Lee, Y.-T., and Chang, Y.-F.: A relationship between Hurst exponents of slip and waiting time data of earthquakes, Physica A, 387, 4643-4648, https://doi.org/10.1016/j.physa.2007.08.063, 2008.

Chen, Y., Ito, Y., Plata-Martinez, R., Dominguez, L. A., Ohyanagi, S., Garcia, E. S., Flores, K., Cruz-Atienza, V. M., Shinohara, M., and Yamashita., Y.: New insight into slow earthquake activities from continuous ocean bottom seismometers at the Guerrero seismic gap, Mexico, Geophys. J. Int., 241, 511-525, https://doi.org/10.1093/gji/ggaf057, 2025.

Cisternas, A., Polat, O., and Rivera, L.: The Marmara Sea region: Seismic behaviour in time and the likelihood of another large earthquake near Istanbul (Turkey), J. Seismol., 8, 427-437, https://doi.org/10.1023/B:JOSE.0000038451.04626.18, 2004.

Corral, A.: Dependence of earthquake recurrence times and independence of magnitudes on seismicity

https://doi.org/10.5194/egusphere-2025-4869
Preprint. Discussion started: 15 December 2025

history, Tectonophysics, 424, 177-193, https://doi.org/10.1016/j.tecto.2006.03.035, 2006.

Cruz-Atienza, V. M., Husker, A., Legrand, D., Caballero, E., and Kostoglodov, V.: Nonvolcanic tremor locations and mechanisms in Guerrero, Mexico, from energy-based and particle motion polarization analysis, J. Geophys. Res., 120, 275-289, https://doi.org/10.1002/2014JB011389, 2015.

Davidsen, J., and Kwiatek, G.: Earthquake interevent time distribution for induced micro-, nano-, and picoseismicity, Phys. Rev. Lett., 110, 1-5, https://doi.org/10.1103/PhysRevLett.110.068501, 2013.

DeMets, C., Gordon, R., Argus, D., and Stein, S.: Effect of recent revisions to the geomagnetic reversal time scale on estimates of current plate motions, Geophys. Res. Lett., 21, 2191-2194, http://dx.doi.org/10.1029/94GL02118, 1994.

De Freitas, D. B., and De Medeiros, J. R.: Nonextensivity in the solar magnetic activity during the increasing phase of the solar cycle 23, EPL, 88, 19001, https://doi.org/10.1209/0295-5075/88/19001, 2009.

De Freitas, D. B., França, G. S., Scherrer, T. M., Vilar, C. S., Silva, R.: Nonextensive triplet in a geological faults system, EPL, 102, 39001, https://doi.org/10.1209/0295-5075/102/39001, 2013.

De Freitas, D. B., and França, G. S.: Analyzing the intrinsic multifractal nature of seismic sequences distributed along the Pacific Ring of Fire, EPL, 146, 60002, https://doi.org/10.1209/0295-5075/ad5101, 2024.

https://doi.org/10.5194/egusphere-2025-4869
Preprint. Discussion started: 15 December 2025

Gallego, A., Russo, R. M., Comte, D., Mocanu, V., Murdie, R. E., VanDecat, J. C.: Tidal modulation of continuous nonvolcanic seismic tremor in the Chile triple junction region, Geochem. Geophy. Geosy., 14, 851-863, https://doi.org/10.1002/ggge.20091, 2013.

Gkarlaouni, C., Lasocki, S., Papadimitriou, E., and George, T.: Hurst analysis of seismicity in Corinth rift and Mygdonia graben (Greece), Chaos Soliton. Fract., 96, 30-42, https://doi.org/10.1016/j.chaos.2017.01.001, 2017.

Gomberg, J., Wech, A., Creager, K., Obara, K., and Agnew, D.: Reconsidering earthquake scaling. Geophys. Res. Lett., 43, 6243-6251, https://doi.org/10.1002/2016GL069967, 2016a.

Gomberg, J., Agnew, D. C., and Schwartz, S. Y.: Alternative source models of very low frequency events, J. Geophys. Res., 121, 6722-6740, https://doi.org/10.1002/2016JB013001, 2016b.

Gu, G-F., and Zhou, W-X.: Detrend moving average algorithm for multifractals, Phys. Rev. E, 82, 011136, https://doi.org/10.1103/PhysRevE.82.011136, 2010.

Gutenberg, B., and Richter, C. F.: Frequency of earthquakes in California, Bull. Seism. Soc. Am., 34, 185-188, https://doi.org/10.1785/BSSA0340040185, 1944.

Hampson, K. M., Mallen, E. A. H.: Multifractal nature of ocular aberration dynamics of the human eye, Biomedical Optics Express, 2, 464, https://doi.org/10.1364/BOE.2.000464, 2011.

Hayes, G. P., Wald, D. J., and Johnson, R. L.: Slab1.0: a three-dimensional model of global subduction

https://doi.org/10.5194/egusphere-2025-4869
Preprint. Discussion started: 15 December 2025

zone geometries, J. Geophys. Res., 117, B01302, https://doi.org/10.1029/2011JB008524, 2012.

Henderson, J., Main, I. G., Pearce, R. G., and Takeya, M.: Seismicity in north-eastern Brazil—Fractal clustering and the evolution of the *b*-value, Geophys. J. Int., 116, 217-226, https://doi.org/10.1111/j.1365-246X.1994.tb02138.x, 1994.

Hurst, E. E.: Long-term storage capacity of reservoirs, T. Am. Soc. Civ. Eng., 116, 770-808, 1951.

Husker, A., Frank, W. B., Gonzalez, G., Avila, L., Kostoglodov, V., and Kazachkina, E.: Characteristic tectonic tremor activity observed over multiple slow slip cycles in the Mexican subduction zone, J. Geophys. Res., 124, 599-608, https://doi.org/10.1029/2018JB016517, 2019.

Ide, S.: Variety and spatial heterogeneity of tectonic tremor worldwide, J. Geophys. Res., 117, B03302, https://doi.org/10.1029/2011JB008840, 2012.

Idehara, K., Yabe, S., and Ide, S.: Regional and global variations in the temporal clustering of tectonic tremor activity, Earth Planets. Sp., 66, 66, https://doi.org/10.1186/1880-5981-66-66, 2014.

Ihlen, E. A. F.: Introduction to multifractal detrended fluctuation analysis in Matlab, Front. Physiol., 3, 141, https://doi.org/10.3389/fphys.2012.00141, 2012.

Jiang Z.-Q., Xie, W.-J., Zhou, W.-X., and Sornette, D.: Multifractal analysis of financial markets, Rep. Prog. Phys., 82, 125901, https://doi.org/10.1088/1361-6633/ab42fb, 2019.

https://doi.org/10.5194/egusphere-2025-4869
Preprint. Discussion started: 15 December 2025

Kantelhardt, J. W., Zschiegner, S. A., Koscielny-Bunde, E., Havlin, S., Bunde, A., and Stanley, H. E.: Multifractal detrended fluctuation analysis of nonstationary time series, Physica A, 316, 87-114, https://doi.org/10.1016/S0378-4371(02)01383-3, 2002.

Kantelhardt, J.W.: Fractal and multifractal time series. In: Meyers, R. (eds) Encyclopedia of Complexity and Systems Science. Springer, New York, NY. https://doi.org/10.1007/978-0-387-30440-3_221, 2009.

Kao, H., Wang, K., Dragert, H., Kao, J. Y., and Rogers, G.: Estimating seismic moment magnitude (M_W) of tremor bursts in northern Cascadia: Implications for the "seismic efficiency" of episodic tremor and slip, Geophys. Res. Lett., 37, L19306, https://doi.org/10.1029/2010GL044927, 2010.

Lay, T., and Wallace, T.: Modern global seismology. ISBN: 012732870X, pp 521., 1995.

Leontitsis, A.: Chaotic Systems Toolbox. Code available at https://github.com/nmitrou/Simulations/tree/master/matlab_codes, 2001.

Mesimeri, M., Karakostas, V., Papadimitriou, E., and Tsaklidis, G.: Characteristics of earthquake clusters: Application to western Corinth Gulf (Greece), Tectonophysics, 767, 228160, https://doi.org/10.1016/j.tecto.2019.228160, 2019.

Mesimeri, M.: Qks_statistics: Utils for earthquake statistics. Code available at https://github.com/mmesim/qks_statistics, 2021.

https://doi.org/10.5194/egusphere-2025-4869
Preprint. Discussion started: 15 December 2025

Michas, G., Sammonds, P., and Vallianatos, F.: Dynamic multifractality in earthquakes time series: insights from Corinth Rift, Greece, Pure Appl. Geophys., 172, 1909-1921, https://doi.org/10.1007/s00024-014-0875-y, 2015.

Miyazawa, M., and Mori, J.: Detection of triggered deep low-frequency events from the 2003 Tokachi-oki earthquake, Geophys. Res. Lett., 32, L10307, https://doi.org/10.1029/2005GL022539, 2005.

Mogi, K.: Some discussions on aftershocks, foreshocks and earthquake swarms: The fracture of a semi-infinite body caused by an inner stress origin and its relation to the earthquake phenomena, Bull. Earthq. Res. Inst., 41, 615-658, 1963.

Nadeau, R. M., and Dolenc, D.: Nonvolcanic tremors deep beneath the San Andreas Fault, Science, 307, 389, https://doi.org/10.1126/science.1107142, 2005.

Nishikawa, T., and Ide, S.: Earthquake size distribution in subduction zones linked to slab buoyancy, Nature Geosci., 7, 904-908, https://doi.org/10.1038/ngeo2279, 2014.

Obara, K.: Nonvolcanic deep tremor associated with subduction in southwest Japan, Science, 296, 1679-1681, https://doi.org/10.1126/science.107037, 2002.

Pardo, M., and Suárez, G.: Shape of the subducted Rivera and Cocos plates in southern Mexico: Seismic and tectonic implications, J. Geophys. Res., 100, 12357-12373, https://doi.org/10.1029/95JB00919, 1995.

https://doi.org/10.5194/egusphere-2025-4869
Preprint. Discussion started: 15 December 2025

Passarelli, L., Hainzl, S., Cesca S., Maccaferri, F., Mucciarelli, M., Roessler, D., Corbi, F., and Dahm, T.: Aseismic transient driving the swarm-like seismic sequence in the Pollino range, Southern Italy, Geophys. J. Int., 201, 1553-1567, https://doi.org/10.1093/gji/ggv111, 2015.

Payero, J. S., Kostoglodov, V., Shapiro, N., Mikumo, T., Iglesias, A., Pérez-Campos, X., and Clayton, R. W.: Nonvolcanic tremor observed in the Mexican subduction zone, Geophys. Res. Lett., 35, L07305, https://doi.org/10.1029/2007GL032877, 2008.

Peacock, S. M.: Thermal and metamorphic environment of subduction zone episodic tremor and slip, J. Geophys. Res., 114, B00A07, https://doi.org/10.1029/2008JB005978, 2009.

Pérez-Campos, X., Kim, Y. H., Husker, A., Davis, P. M., Clayton, R. W., Iglesias, A., Pacheco, J. F., Singh, S. K., Manea, V. C., and Gurnis, M.: Horizontal subduction and truncation of the Cocos Plate beneath central Mexico, Geophys. Res. Lett., 35, L18303, https://doi.org/10.1029/2008GL035127, 2008.

Plata-Martinez, R., Ide, S., Shinohara, M., Garcia, E. S., Mizuno, N., Dominguez, L. A., Taira, T., Yamashita, Y., Toh, A., Yamada, T., Real, J., Husker, A., Cruz-Atienza, V. M., and Ito, Y.: Shallow slow earthquakes to decipher future catastrophic earthquakes in the Guerrero seismic gap, Nat. Commun., 12, 3976, https://doi.org/10.1038/s41467-021-24210-9, 2021.

Post, R. A. J., Michels, M. A. J., Ampuero, J.-P., Candela, T., Fokker, P. A., Van Wees, J.-D., Van der Hofstad, R. W., and Van den Heuvel, E. R.: Interevent time distribution and aftershock frequency in non-stationary induced seismicity, Sci. Rep. 11, 3540, https://doi.org/10.1038/s41598-021-82803-2,

https://doi.org/10.5194/egusphere-2025-4869
Preprint. Discussion started: 15 December 2025

2021.

Rabbel, W., Thorwart, M. M., and Taylor, W.: Non-volcanic tremor in Costa Rica: *b*-values, moment release and tidal modulation, AGU Fall Meeting 2011, Online, 5–9 December 2011, S23B-2245, https://ui.adsabs.harvard.edu/abs/2011AGUFM.S23B2245R/abstract, 2011.

Rogers, G., and Dragert, H.: Episodic tremor and slip on the Cascadia subduction zone: the chatter of silent slip, Science, 300, 1942-19443, https://doi.org/10.1126/science.108478, 2003.

Rubinstein, J. L., Vidale, J. E., Gomberg, J., Bodin, P., Creager, K. C., and Malone, S. D.: Non-volcanic tremor driven by large transient shear stresses, Nature, 448, 579-582, https://doi.org/10.1038/nature06017, 2007.

Saichev, A., Sornette, D.: Generic multifractality in exponentials of long memory processes, Phys. Rev. E, 74, 011111, http://dx.doi.org/10.1103/PhysRevE.74.011111, 2006.

Sarlis, N. V., Skordas, E. S., and Varotsos, P. A.: Nonextensivity and natural time: the case of seismicity, Phys Rev E, 82, 021110, http://dx.doi.org/10.1103/PhysRevE.82.021110, 2010.

Scherrer, T. M., França, G. S., Silva, R., de Freitas, D. B., and Vilar, C. S.: Nonextensivity at the Circum-Pacific subduction zones—Preliminary studies, Physica A, 426, 63-71, https://doi.org/10.1016/j.physa.2014.12.038, 2015.

Scholz, C. H.: On the stress dependence of the earthquake *b*-value, Geophys. Res. Lett., 42, 1399-1402,

https://doi.org/10.5194/egusphere-2025-4869
Preprint. Discussion started: 15 December 2025

https://doi.org/10.1002/2014GL062863, 2015.

Schorlemmer, D., Wiemer, S., and Wyss, M.: Variations in earthquake-size distribution across different stress regimes, Nature, 437, 539-542, https://doi.org/10.1038/nature04094, 2005.

Schreiber, T., and Schmitz, A.: Improved surrogate data for nonlinearity tests, Phys. Rev. Lett., 77, 635-638, https://doi.org/10.1103/PhysRevLett.77.635, 1996.

Schreiber, T., and Schmitz, A.: Surrogate time series, Physica D: Nonlinear Phenomena, 142, 346-382, https://doi.org/10.1016/S0167-2789(00)00043-9, 2000.

Schwartz, S. Y., Rokosky, J. M.: Slow slip events and seismic tremor at circum-Pacific subduction zones, Rev. Geophys., 45, RG3004, https://doi.org/10.1029/2006RG000208, 2007.

Shelly, D. R., Beroza, G. C., Ide, S., and Nakamula, S.: Low-frequency earthquakes in Shikoku, Japan, and their relationship to episodic tremor and slip, Nature, 442, 188-191, https://doi.org/10.1038/nature04931, 2006.

Shelly, D. R., Beroza, G. C., and Ide, S.: Non-volcanic tremor and low-frequency earthquake swarms, Nature, 446, 305-307, https://doi.org/10.1038/nature05666, 2007.

Shelly, D. R.: Migrating tremor illuminates deformation beneath the seismogenic San Andreas fault, Nature, 463, 648-652, https://doi.org/10.1038/nature08755, 2010.

https://doi.org/10.5194/egusphere-2025-4869
Preprint. Discussion started: 15 December 2025

Silva, R., Franca, G. S., Vilar, C. S., and Alcaniz, J. S.: Nonextensive models for earthquakes, Phys. Rev. E, 7, 026102, http://dx.doi.org/10.1103/PhysRevE.73.026102, 2006.

Singh, S. K., and Mortera, F.: Source time functions of large Mexican subduction earthquakes, morphology of the Benioff Zone, age of the plate, and their tectonic implications, J. Geophys. Res., 96, 21487-21502, https://doi.org/10.1029/91JB02047, 1991.

Solotongo-Costa, O., and Posadas, A.: Fragment-asperity interaction model for earthquakes, Phys. Rev. Lett., 92, 048501, http://dx.doi.org/10.1103/PhysRevLett.92.048501, 2004.

Staudenmaier, N., Tormann, T., Edwards, B., Mignan, A., and Wiemer, S.: The frequency-size scaling of non-volcanic tremors beneath the San Andreas Fault at Parkfield: Possible implications for seismic energy release, Earth Planet. Sci. Lett., 516, 77-107, https://doi.org/10.1016/j.epsl.2019.04.006, 2019.

Sweet, J. R., Creager, K. C., and Houston, H.: A family of repeating low-frequency earthquakes at the downdip edge of tremor and slip, Geochem. Geophys. Geosyst., 15, 3713-3721, https://doi.org/10.1002/2014GC005449, 2014.

Tang, C.-C., Peng, Z., Chao, K., Chen, C.-H., and Lin, C.-H.: Detecting low-frequency earthquakes within non-volcanic tremor in southern Taiwan triggered by the 2005 M_W 8.6 Nias earthquake, Geophys. Res. Lett., 37, L16307, https://doi.org/10.1029/2010GL043918, 2010.

Telesca, L., Cuomo, V., and Lapenna, V.: A new approach to investigate the correlation between geoelectrical time fluctuations and earthquakes in a seismic area of southern Italy, Geophys. Res. Lett.,

https://doi.org/10.5194/egusphere-2025-4869
Preprint. Discussion started: 15 December 2025

28, 4375-4378, https://doi.org/10.1029/2001GL013467, 2001.

Traversa, P., and Grasso, J.-R.: How is volcano seismicity different from tectonic seismicity?, B. Seismol. Soc. Am., 100, 1755-1769, https://doi.org/10.1785/0120090214, 2010.

Tsallis, C.: Introduction to nonestensive statistical mechanics. Approaching a Complex World, Springer, New York, 382pp., 2009.

Villafuerte, C., and Cruz-Atienza, V. M.: Insights into the causal relationship between slow slip and tectonic tremor in Guerrero, Mexico, J. Geophys. Res., 122, 6642-6656, https://doi.org/10.1002/2017JB014037, 2017.

Virtanen, P., Gommers, R., Oliphant, T. E., Haberland, M., Reddy, T., Cournapeau, D., Burovski, E., Peterson, P., Weckesser, W., Bright, J., Van der Walt, S. J., Brett, M., Wilson, J., Millman, K. J., Mayorov, N., Nelson, A. R. J., Jones, E., Kern, R., Larson, E., Carey, C. J., Polat, I., Feng, Y., Moore, E. W., and VanderPlas, J.: SciPy 1.0: Fundamental algorithms for scientific computing in Python. Nat. Methods, 17, 261-272, https://doi.org/10.1038/s41592-019-0686-2, 2020.

Wada, I., Wang, K., He, J., and Hyndman, R. D.: Weakening of the subduction interface and its effects on surface heat flow, slab dehydration, and mantle wedge serpentinization, J. Geophys. Res., 113, B04402, https://doi.org/10.1029/2007JB005190, 2008.

Wang, L., Gao, X.-L., and Zhou, W.-X.: Testing for intrinsic multifractality in the global grain spot market indices: a multifractal detrended fluctuation analysis, Fractals, 31, 2350090,

https://doi.org/10.5194/egusphere-2025-4869
Preprint. Discussion started: 15 December 2025

https://doi.org/10.1142/S0218348X23500901, 2023.

Warren, N. W., and Latham, G. V.: An experimental study of thermally induced microfracturing and its relation to volcanic seismicity, J. Geophys. Res., 75, 4455-4464, https://doi.org/10.1029/JB075i023p04455, 1970.

Wessel , P. , Luis, J. F., Uieda, L. A., Scharroo, R., Wobbe, F., Smith, W. H., Tian, D.: The generic mapping tools version 6, Geochem. Geophys. Geosyst., 20, 5556-5564, https://doi.org/10.1029/2019GC008515, 2019.

Wetzler, N.: Calc_gr_ks.py: A program to calculate the *b*-value Gutenberg-Richter magnitude distribution using the Kolmogorov–Smirnov test. Code available at https://github.com/nadavwetzler/b-value, 2022.

Yoshioka, S., Toda, M., and Nakajima, J.: Regionality of deep low-frequency earthquakes associated with subduction of the Philippine Sea plate along the Nankai Trough, southwest Japan, Earth Planet. Sci. Lett., 272, 189-198, https://doi.org/10.1016/j.epsl.2008.04.039, 2008.

https://doi.org/10.5194/egusphere-2025-4869
Preprint. Discussion started: 15 December 2025

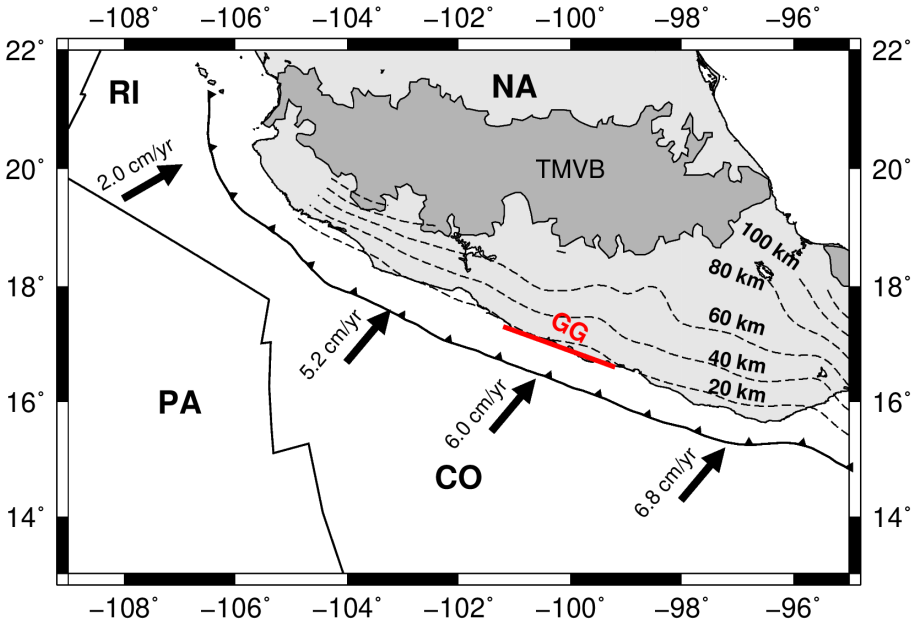

Figure 1. Tectonic framework of the Mexican subduction zone. TMVB is the Trans-Mexican Volcanic Belt. CO, NA, PA, and RI are the Cocos, North American, Pacific, and Rivera plates, respectively. GG is the Guerrero seismic gap. Black arrows indicate the convergence rate among tectonic plates. Dashed lines represent contour lines of the subducted plate, spaced every 20 km, from 20 to 100 km (Hayes, 2012).

https://doi.org/10.5194/egusphere-2025-4869
Preprint. Discussion started: 15 December 2025

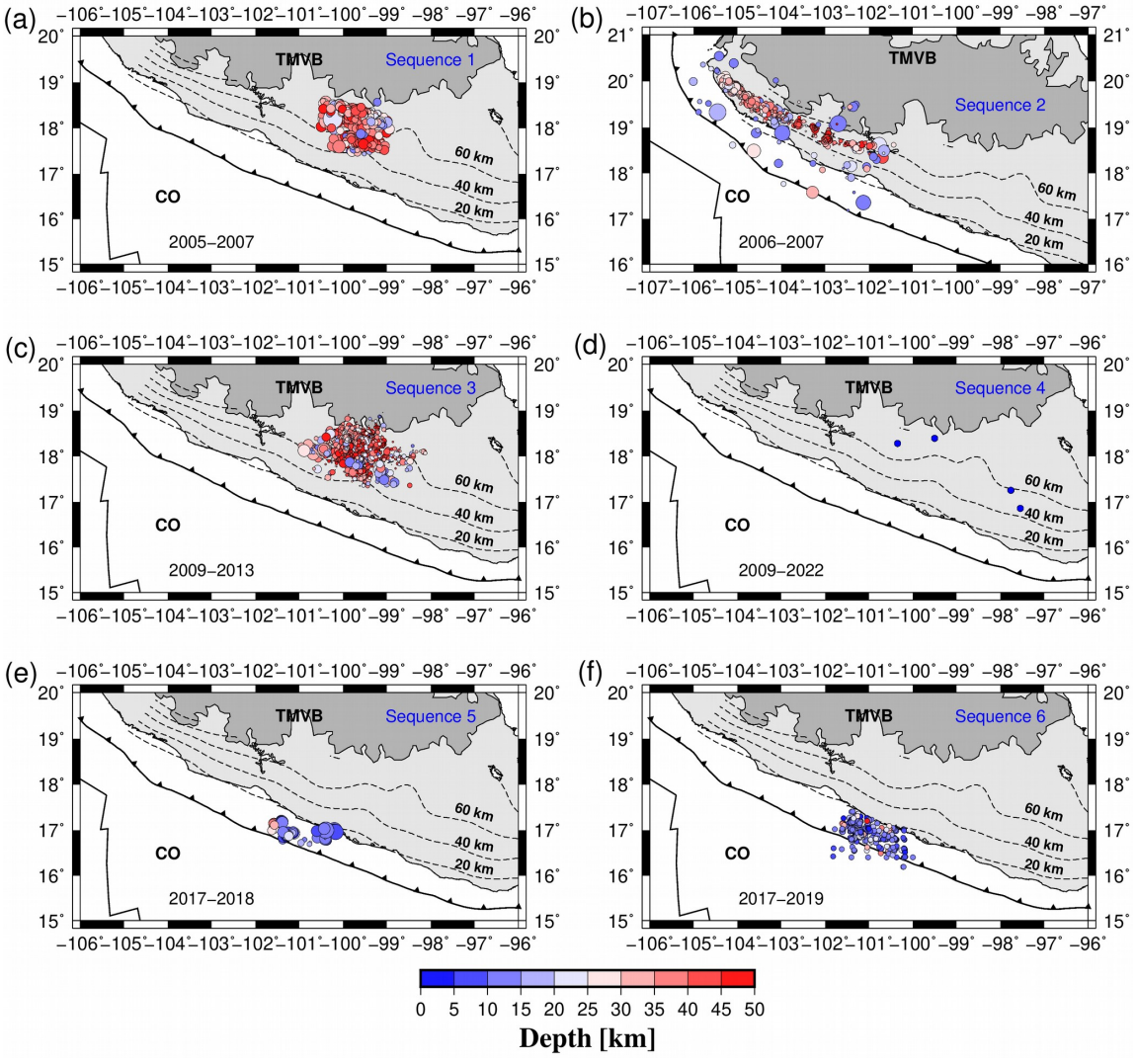

Figure 2. Hypocenter locations of all the studied non-volcanic tremor sequences along the Mexican subduction zone. (**a**) sequence 1, (**b**) sequence 2, (**c**) sequence 3, (**d**) sequence 4, (**e**) sequence 5, and (**f**) sequence 6.

https://doi.org/10.5194/egusphere-2025-4869
Preprint. Discussion started: 15 December 2025

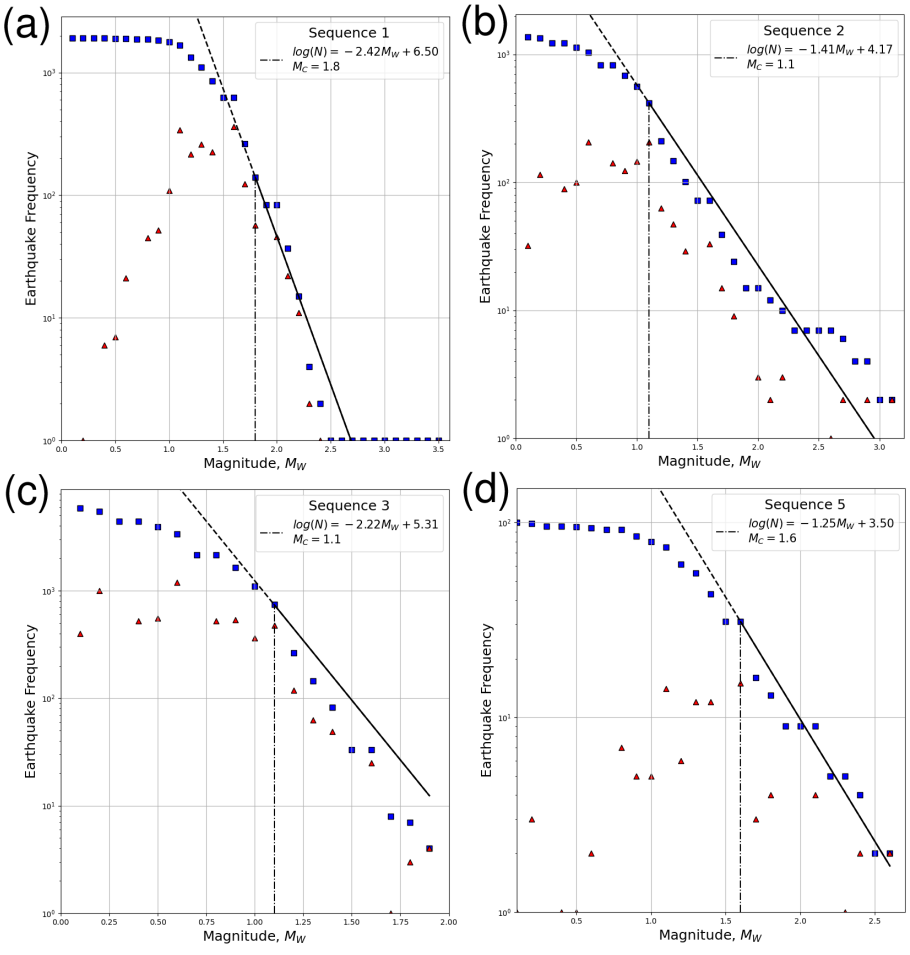

Figure 3. Estimates of *b*-value and M_c for the studied NVT sequences. Blue squares show the cumulative number of events versus magnitude. Red triangles exhibit the number of events. The solid black lines indicate the Gutenberg-Righter frequency magnitude distributions. (**a**) sequence 1, (**b**) sequence 2, (**c**) sequence 3, and (**d**) sequence 5.

https://doi.org/10.5194/egusphere-2025-4869
Preprint. Discussion started: 15 December 2025

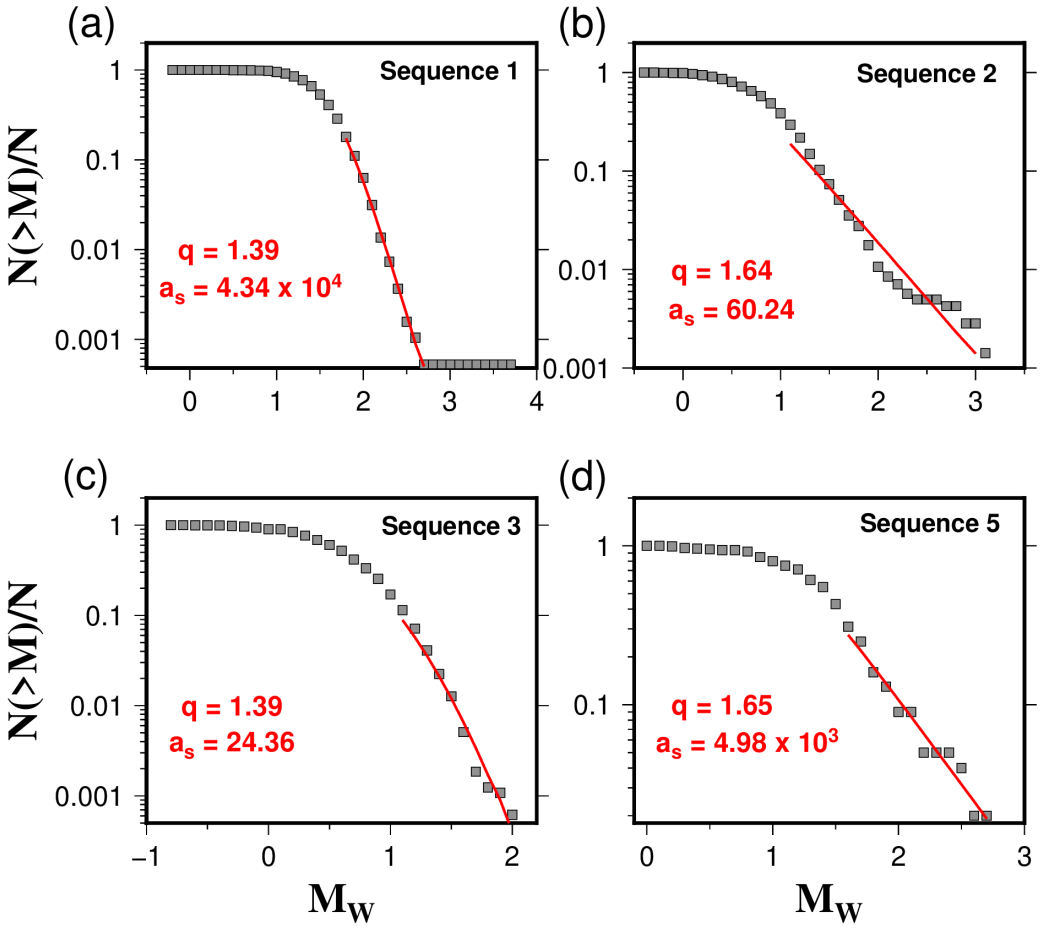

Figure 4. Normalized cumulative number of earthquake with magnitude $m > M_{th}$ and fitting obtained with the fragment asperity model for the seismicity monitored in each NVT sequence. (**a**) sequence 1, (**b**) sequence 2, (**c**) sequence 3, and (**d**) sequence 5.

https://doi.org/10.5194/egusphere-2025-4869
Preprint. Discussion started: 15 December 2025

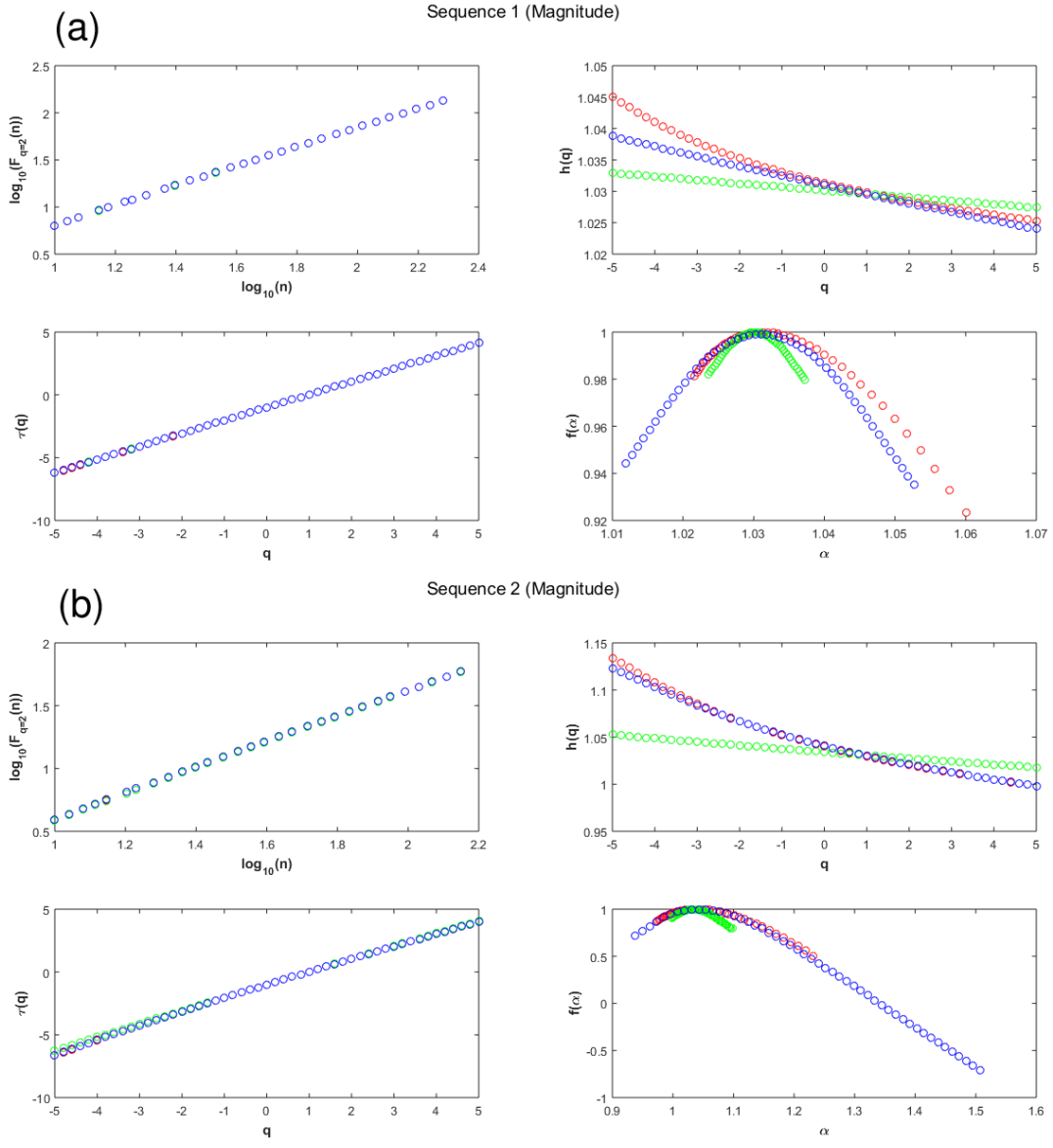

Figure 5. Multifractal analysis of magnitude for sequences 1 (**a**) and 2 (**b**) (fluctuation function, $F(q)$; Hurst exponent, $h(q)$; multifractal scaling exponent $\tau(q)$; and multifractal spectrum $f(\alpha)$). In all cases, the original, shuffled, and IAAFT surrogates data are shown in red, green, and blue color, respectively.

https://doi.org/10.5194/egusphere-2025-4869
Preprint. Discussion started: 15 December 2025

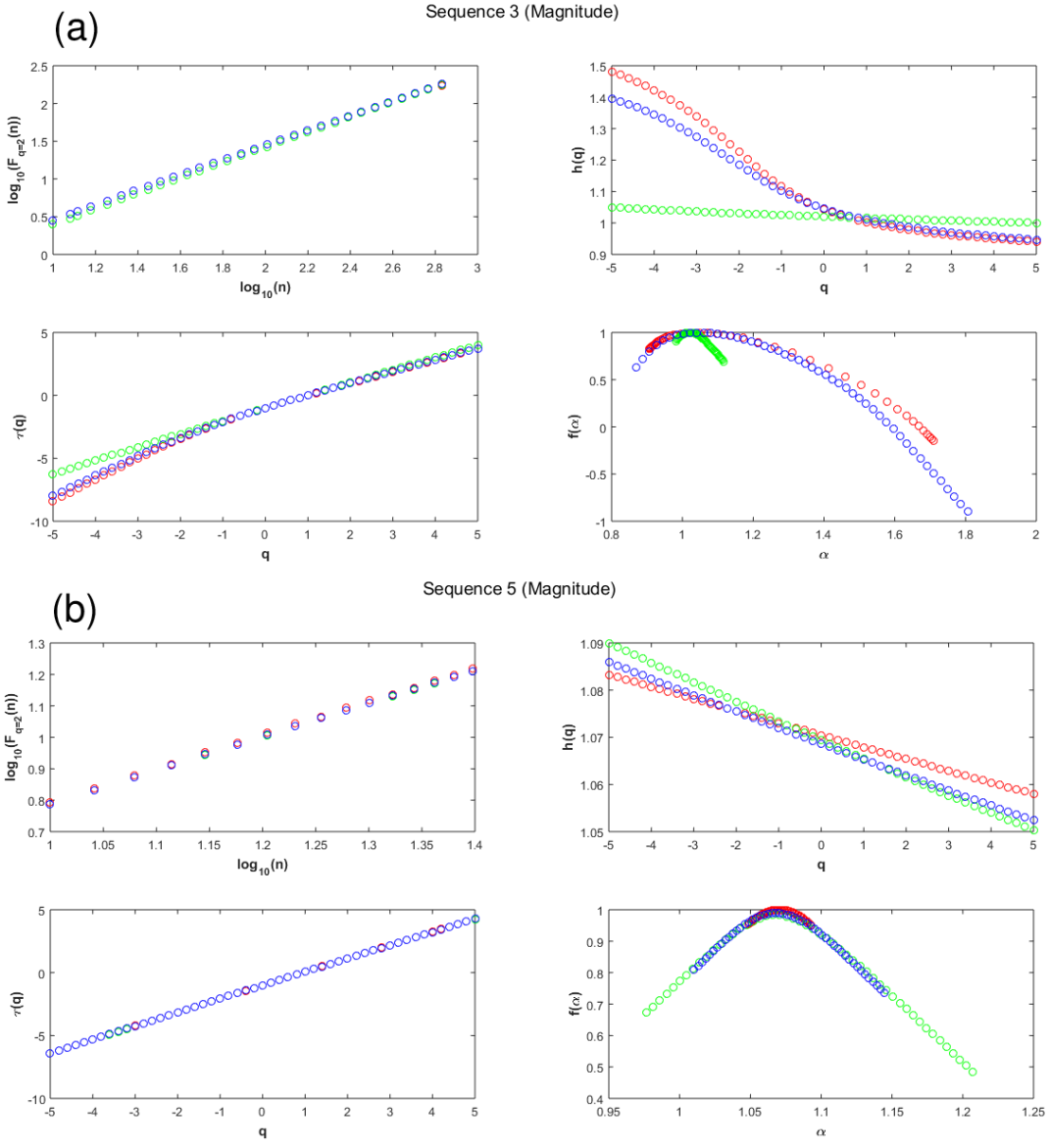

Figure 6. Multifractal analysis of magnitude for sequences 3 (**a**) and 5 (**b**) (fluctuation function, $F(q)$; Hurst exponent, $h(q)$; multifractal scaling exponent $\tau(q)$; and multifractal spectrum $f(\alpha)$). In all cases, the original, shuffled, and IAAFT surrogates data are shown in red, green, and blue color, respectively.

https://doi.org/10.5194/egusphere-2025-4869
Preprint. Discussion started: 15 December 2025

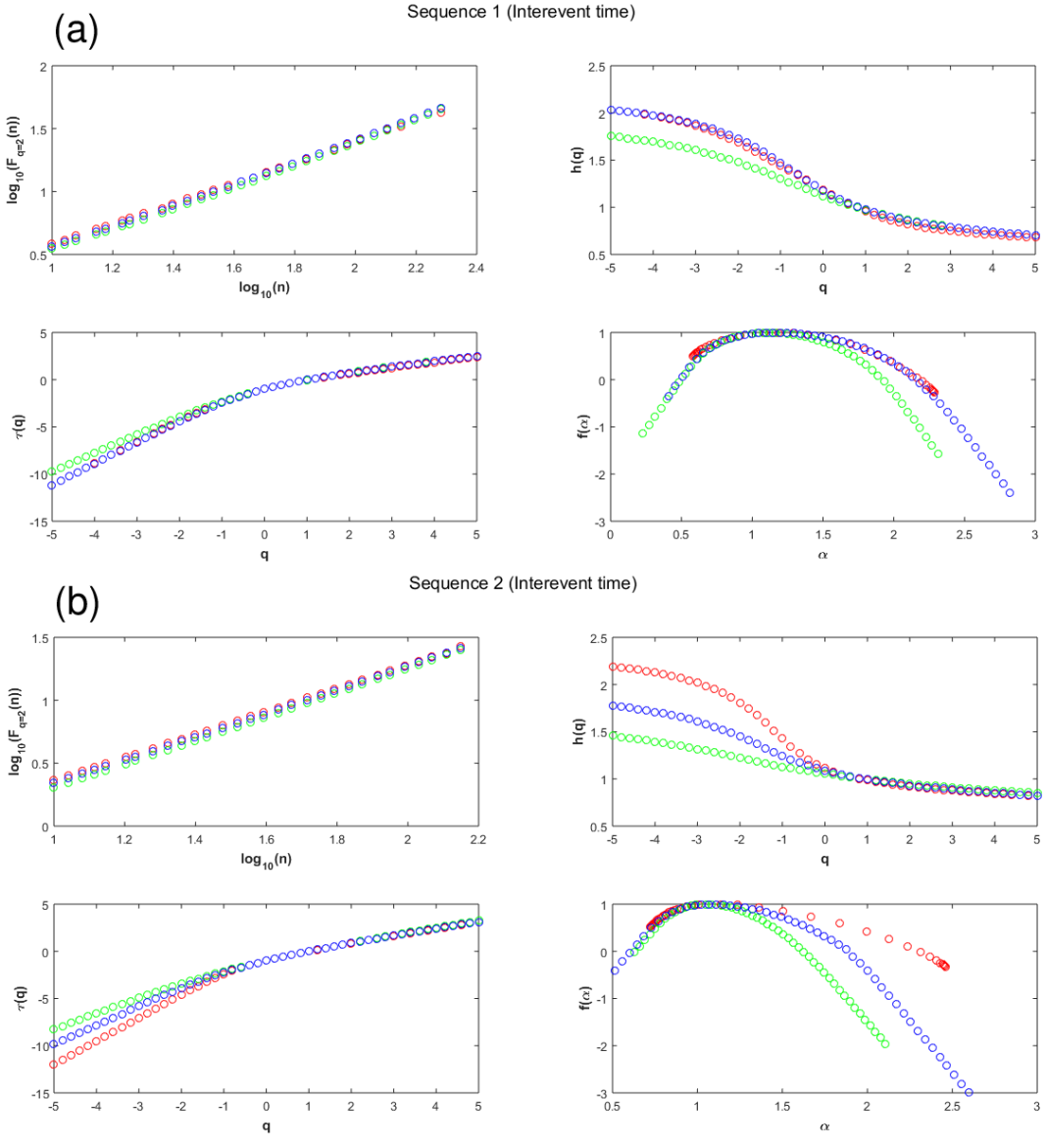

Figure 7. Multifractal analysis of interevent time for sequences 1 (**a**) and 2 (**b**) (fluctuation function, $F(q)$; Hurst exponent, $h(q)$; multifractal scaling exponent $\tau(q)$; and multifractal spectrum $f(\alpha)$). In all cases, the original, shuffled, and IAAFT surrogates data are shown in red, green, and blue color, respectively.

https://doi.org/10.5194/egusphere-2025-4869
Preprint. Discussion started: 15 December 2025

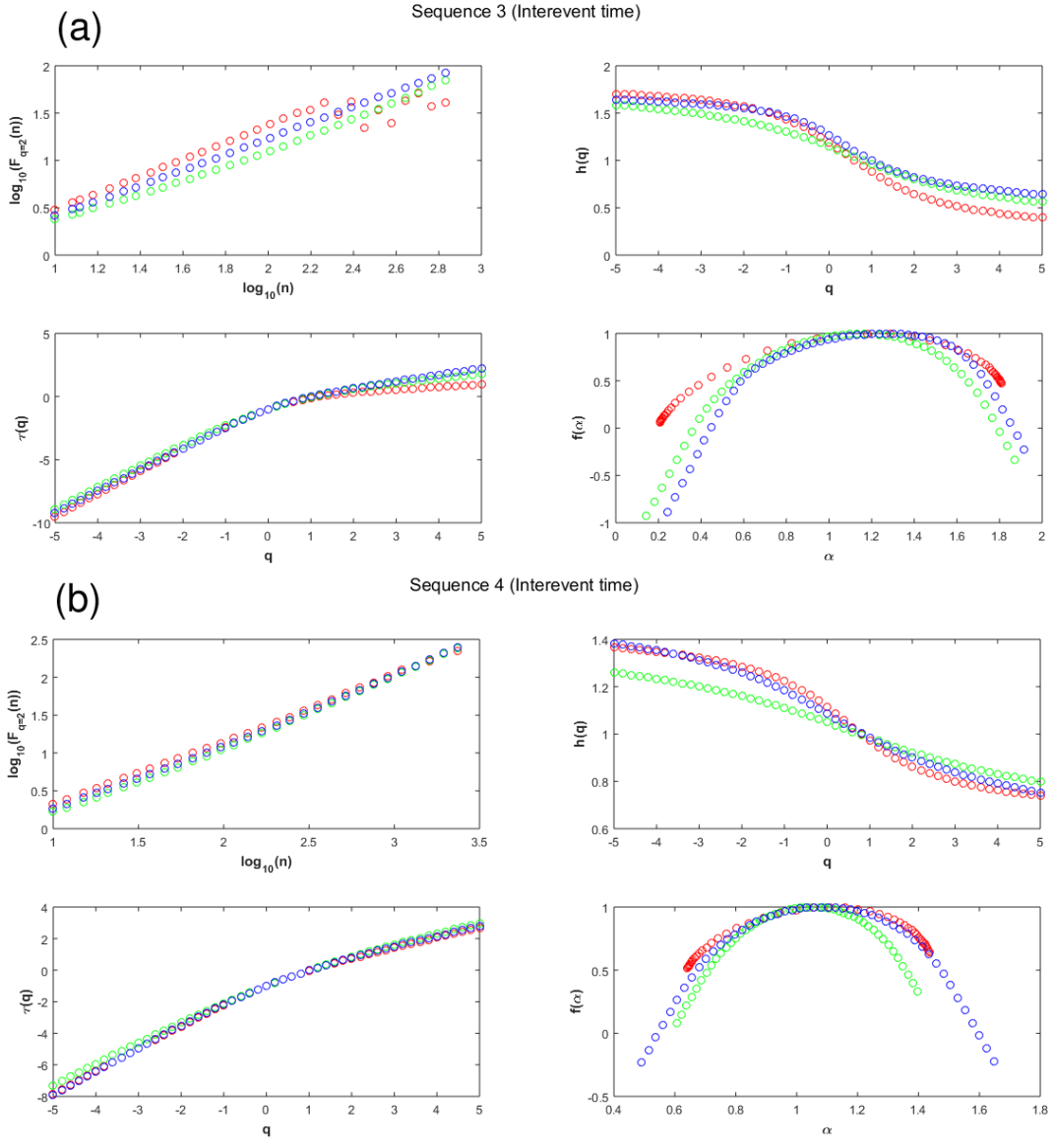

Figure 8. Multifractal analysis of interevent time for sequences 3 (**a**) and 4 (**b**) (fluctuation function, $F(q)$; Hurst exponent, $h(q)$; multifractal scaling exponent $\tau(q)$; and multifractal spectrum $f(\alpha)$). In all cases, the original, shuffled, and IAAFT surrogates data are shown in red, green, and blue color, respectively.

https://doi.org/10.5194/egusphere-2025-4869
Preprint. Discussion started: 15 December 2025

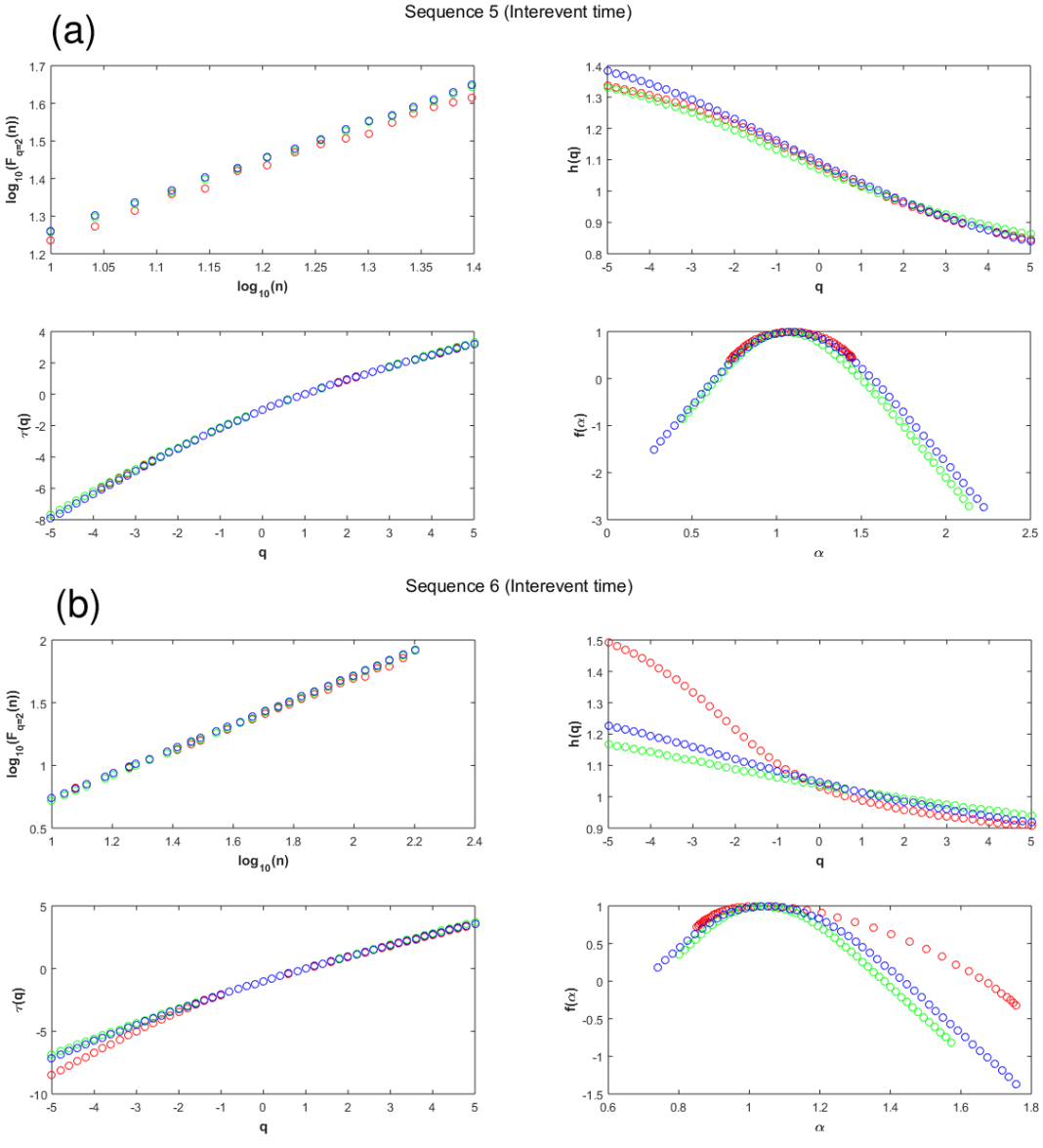

Figure 9. Multifractal analysis of interevent time for sequences 5 (**a**) and 6 (**b**) (fluctuation function, $F(q)$; Hurst exponent, $h(q)$; multifractal scaling exponent $\tau(q)$; and multifractal spectrum $f(\alpha)$). In all cases, the original, shuffled, and IAAFT surrogates data are shown in red, green, and blue color, respectively.

https://doi.org/10.5194/egusphere-2025-4869
Preprint. Discussion started: 15 December 2025

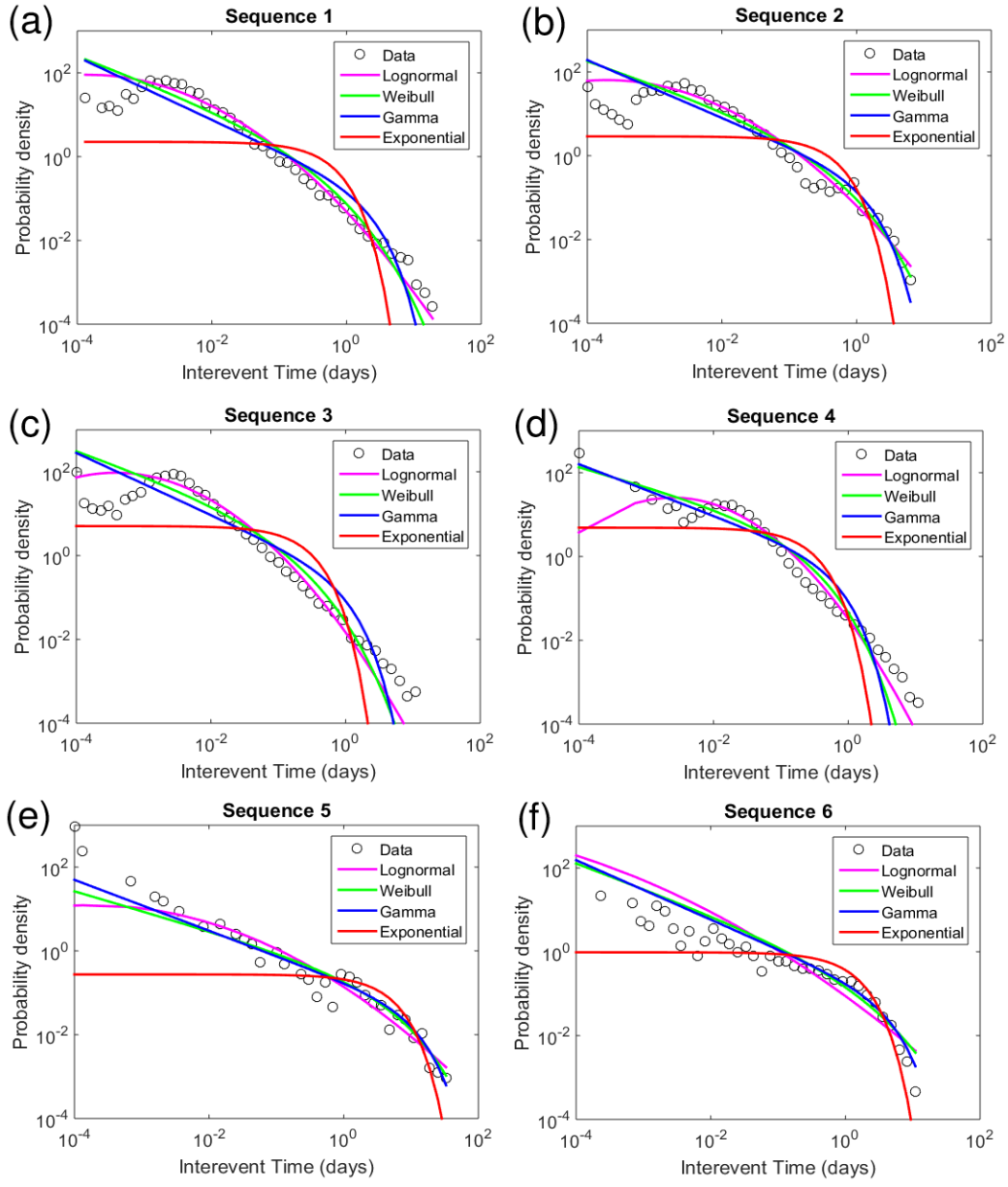

Figure 10. Probability density functions of the interevent times for the NVT sequences and fitted curves of different statistical distributions (exponential, Gamma, Lognormal, and Weibull). (**a**) sequence 1, (**b**) sequence 2, (**c**) sequence 3, (**d**) sequence 4, (**e**) sequence 5, and (**f**) sequence 6.

https://doi.org/10.5194/egusphere-2025-4869
Preprint. Discussion started: 15 December 2025

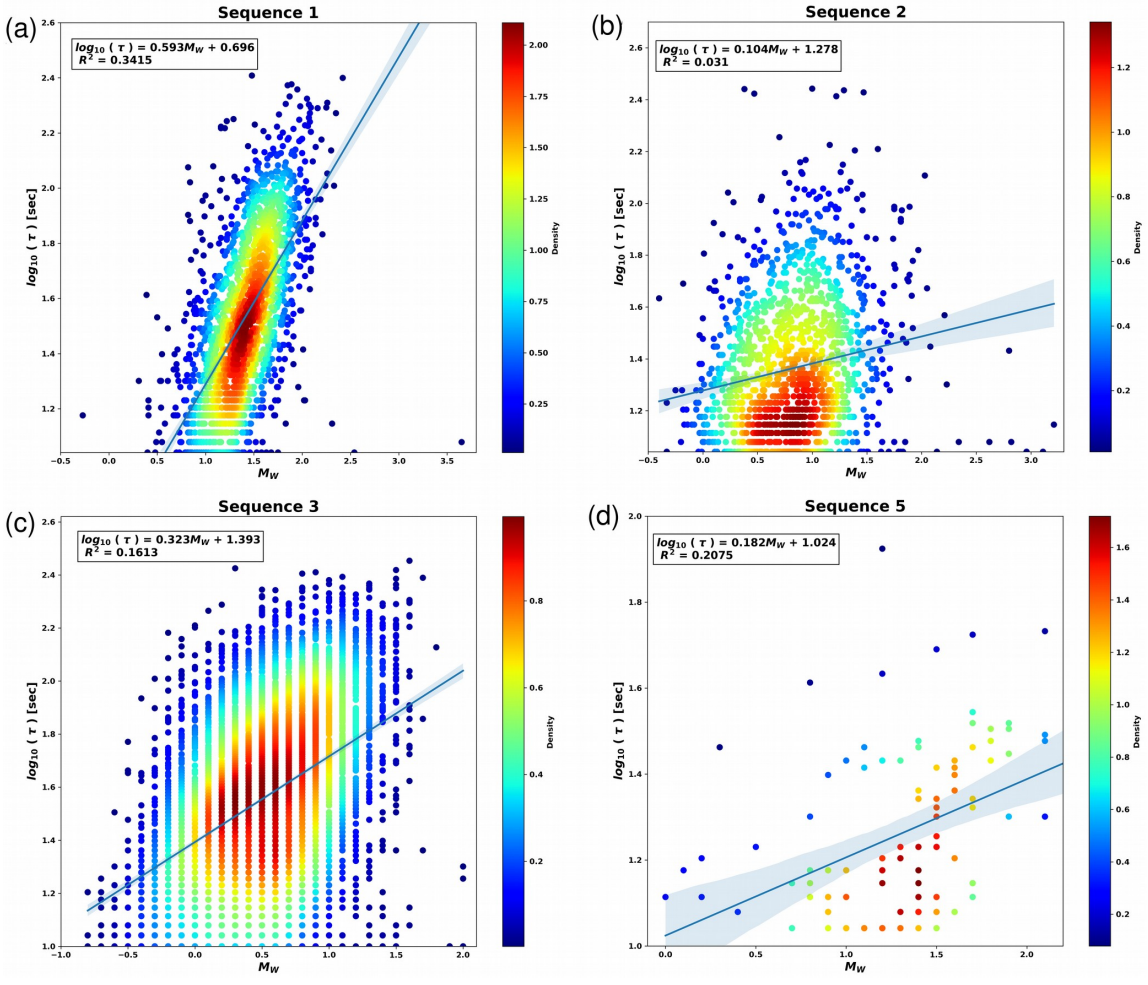

Figure 11. NVT duration scaling relationships (blue lines). In all figures, color indicates the density of NVT observations. (**a**) sequence 1, (**b**) sequence 2, (**c**) sequence 3, and (**d**) sequence 5.

https://doi.org/10.5194/egusphere-2025-4869
Preprint. Discussion started: 15 December 2025

Table 1. Studied non-volcanic tremor sequences. N is the number of events; M_W is the moment magnitude; T_1 and T_2 are the start and end dates of the located NVTs.

Sequence	N	T_1 yyyy/mm/dd	T_2 yyyy/mm/dd	M_W	Reference
1	1908	2005/01/14	2007/05/28	-0.27 – 3.65	Ide (2012), Idehara et al. (2014)
2	1411	2006/01/26	2007/06/06	-0.40 – 3.21	Ide (2012), Idehara et al. (2014)
3	6776	2009/11/26	2013/08/11	-0.80 – 2.00	Ide (2012), Idehara et al. (2014)
4	23408	2009/03/04	2022/05/29		Husker et al. (2019)
5	101	2017/11/22	2018/11/12	0.10 – 2.70	Plata-Martínez et al. (2021)
6	637	2017/11/21	2019/09/10		Chen et al. (2025)

Table 2. Results for the Gutenberg-Richter relationship.

Sequence	b-value	a-value	M_c
1	2.42	6.50	1.80
2	1.41	4.17	1.10
3	2.22	5.31	1.10
5	1.25	3.50	1.60

Table 3. Results for the fragment asperity model.

Sequence	q-value	a_s-value
1	1.39	4.34×10^4
2	1.64	60.24
3	1.39	24.36
5	1.65	4.98×10^3

Table 4. Testing multifractality of multifractal parameters. M_W is the moment magnitude; Δt is the interevent times; A is the degree of asymmetry; $\Delta\alpha$ is the degree of multifractality; Δf is the singularity parameter; and H is the Hurst index. The symbol $\langle\rangle$ denotes the mean and σ indicates the standard deviation. The p-values represent the proportion of IAAFT surrogates measured for each indicator that exceeds the index's value for the original time series.

Parameter	Sequence	A	$\langle A \rangle$	σ_A	p-value	$\Delta\alpha$	$\langle \Delta\alpha \rangle$	$\sigma_{\Delta\alpha}$	p-value	Δf	$\langle \Delta f \rangle$	$\sigma_{\Delta f}$	p-value	H	$\langle H \rangle$	σ_H	p-value
M_W	1	2.96	1.16	0.14	0.00	0.04	0.03	0.002	0.00	-0.060	-0.006	0.005	0.00	1.03	1.03	0.002	0.47
	2	2.83	2.31	1.06	0.25	0.26	0.23	0.070	0.25	-0.370	-0.254	0.203	0.77	1.02	1.02	0.006	0.58
	3	4.67	3.91	0.43	0.05	0.80	0.69	0.061	0.05	-0.980	-0.822	0.118	0.91	0.98	0.99	0.005	0.94
	5	1.04	1.11	0.29	0.56	0.04	0.06	0.014	0.83	-0.002	-0.007	0.022	0.43	1.06	1.06	0.012	0.39
Δt	1	1.82	1.73	0.36	0.42	1.71	1.70	0.204	0.50	-0.780	-0.452	0.311	0.85	0.82	0.86	0.016	0.99
	2	3.16	2.48	0.66	0.14	1.73	1.32	0.194	0.03	-0.810	-0.724	0.289	0.62	0.92	0.93	0.015	0.80
	3	0.65	0.62	0.13	0.43	1.60	1.23	0.128	0.00	0.413	0.312	0.203	0.34	0.65	0.83	0.025	0.00
	4	0.70	0.88	0.09	0.96	0.80	0.89	0.050	0.98	0.125	0.129	0.132	0.49	0.86	0.90	0.004	0.00
	5	1.02	1.32	0.79	0.58	0.72	0.84	0.256	0.65	0.031	-0.122	0.490	0.41	0.96	0.97	0.060	0.61
	6	3.90	1.49	0.58	0.00	0.90	0.50	0.090	0.00	-1.044	-0.210	0.224	0.99	0.96	0.99	0.021	0.86

https://doi.org/10.5194/egusphere-2025-4869
Preprint. Discussion started: 15 December 2025

Table 5. Estimated parameters for the PDF of interevent times. AIC and BIC are the Akaike and Bayesian information criteria; *D* is the test statistic.

Sequence	Distribution	Parameters	-logL	K-S test *p*-value	K-S test *D*	AIC	BIC
1	Lognormal	μ = -3.65 σ = 2.27	-2696	0.70	0.10	-5389	-5385
	Weibull	α = 0.09 b = 0.40	-2399	0.31	0.14	-4795	-4791
	Gamma	α = 0.25 b = 1.78	-2020	0.02	0.23	-4036	-4033
	Exponential	μ = 0.44	359	2.50×10^{-13}	0.58	719	721
2	Lognormal	μ = -3.26 σ = 2.30	-1424	0.83	0.09	-2845	-2841
	Weibull	α = 0.12 b = 0.44	-1308	0.39	0.14	-2611	-2608
	Gamma	α = 0.31 b = 1.11	-1191	0.08	0.20	-2378	-2375
	Exponential	μ = 0.35	84	3.81×10^{-9}	0.48	-166	-164
3	Lognormal	μ = -4.34 σ = 1.88	-15527	0.41	0.13	-31051	-31047
	Weibull	α = 0.04 b = 0.44	-14009	0.09	0.18	-28014	-28011
	Gamma	α = 0.26 b = 0.76	-12035	0.0009	0.28	-24066	-24062
	Exponential	μ = 0.20	-4202	2.58×10^{-16}	0.61	-8402	-8400
4	Lognormal	μ = -3.30 σ = 1.64	-32533	0.62	0.12	-65063	-65059
	Weibull	α = 0.09 b = 0.54	-28883	0.18	0.17	-57762	-57759
	Gamma	α = 0.38 b = 0.53	-24665	0.0064	0.27	-49326	-49323
	Exponential	μ = 0.20	-13681	2.09×10^{-8}	0.48	-27359	-27358
5	Lognormal	μ = -0.39 σ = 2.86	208	0.07	0.22	419	423
	Weibull	α = 2.25 b = 0.53	188	0.47	0.14	382	384
	Gamma	α = 0.39 b = 9.30	185	0.68	0.12	374	377
	Exponential	μ = 3.65	229	0.05	0.23	461	462
6	Lognormal	μ = -2.35 σ = 3.74	246	0.07	0.21	495	499
	Weibull	α = 0.49 b = 0.40	139	0.26	0.16	283	286
	Gamma	α = 0.29 b = 3.54	76	0.42	0.14	156	159
	Exponential	μ = 1.03	655	0.01	0.25	1312	1314

https://doi.org/10.5194/egusphere-2025-4869
Preprint. Discussion started: 15 December 2025

Table 6. Duration scaling relationships ($\log(\tau) = a + b\,M_W$). R^2 is the determination coefficient; b is the slope and a is the intercept.

Sequence	a	b	R^2
1	0.696	0.593	0.341
2	1.278	0.104	0.031
3	1.393	0.323	0.161
5	1.024	0.182	0.208